

Article

Concentration Dependent Improved Spectroscopic Characteristics and Near White Light Emission in Boro Phosphate Glasses Doped with Holmium

Sajid Ali Ansari ^{1,*} , Mohammad Omaish Ansari ² , Ahmed Alshahrie ^{2,3}, Mohammad Shahadat ⁴, Nazish Parveen ⁵, Reem Darwesh ³ and Samia Faisal Aboushoushah ³

¹ Department of Physics, College of Science, King Faisal University, P.O. Box 400, Hofuf 31982, Al-Ahsa, Saudi Arabia

² Center of Nanotechnology, King Abdulaziz University, Jeddah 21589, Saudi Arabia; moansari@kau.edu.sa (M.O.A.); aalshahri@kau.edu.sa (A.A.)

³ Department of Physics, King Abdulaziz University, Jeddah 21589, Saudi Arabia; rdarwesh@kau.edu.sa (R.D.); saboushoushah@kau.edu.sa (S.F.A.)

⁴ School of Chemical Sciences, Universiti Sains Malaysia, Pulau Pinang 11800, Malaysia; mdshahadat@usm.my

⁵ Department of Chemistry, College of Science, King Faisal University, P.O. Box 380, Hofuf 31982, Al-Ahsa, Saudi Arabia; nislam@kfu.edu.sa

* Correspondence: sansari@kfu.edu.sa; Tel.: +966-13-589-9598

Abstract: The physical, structural, thermal, and optical properties of heavy metal (Ho^{3+}) oxide incorporated lithium-boro-phosphate glass prepared utilizing melt quenching process are presented in this paper as a function of dopant concentration. To support the findings of the FTIR and DSC studies, many theoretical, experimental, physical, and optical parameters were calculated. XRD and FTIR measurements revealed the prepared glasses' amorphous nature and the presence of significant borate functional groups. The optical band gap, Urbach energy, and steepness characteristics were tested to validate the structural results. The emission spectrums were recorded in the prepared glasses for an excitation of 450 and 550 nm to find powerful emission color. The color co-ordinates (0.33, 0.41) were found to be quite comparable to white light color co-ordinates. The present glasses can, therefore, be ideal candidates for possible applications with light-emitting diodes.

Keywords: holmium-doped glasses; emission; heavy metal oxide; UV-Vis-NIR; melt quenching



Citation: Ansari, S.A.; Ansari, M.O.; Alshahrie, A.; Shahadat, M.; Parveen, N.; Darwesh, R.; Aboushoushah, S.F. Concentration Dependent Improved Spectroscopic Characteristics and Near White Light Emission in Boro Phosphate Glasses Doped with Holmium. *Appl. Sci.* **2022**, *12*, 2632. <https://doi.org/10.3390/app12052632>

Academic Editors: Zhenxu Bai, Qiang Wu and Quan Sheng

Received: 17 January 2022

Accepted: 25 February 2022

Published: 3 March 2022

Publisher's Note: MDPI stays neutral with regard to jurisdictional claims in published maps and institutional affiliations.



Copyright: © 2022 by the authors. Licensee MDPI, Basel, Switzerland. This article is an open access article distributed under the terms and conditions of the Creative Commons Attribution (CC BY) license (<https://creativecommons.org/licenses/by/4.0/>).

1. Introduction

The use of glasses in various industries, including displays, lasers, optical fibers, upgrading converters, photonics and medicine, has been growing in everyday life in recent years [1–3]. Borate and phosphate are the most frequent glass-tech network formers because they offer beneficial physical qualities for the formation of glass, such as a low temperature of glass transition, a low melting point, and a high refractive index [3,4]. In addition, it has been found to boost glass chemical stability by combining both network formers. Mixed glass formers (MGFs) of alkaline and alkaline such as boro-phosphates [4,5], borosilicates [6,7], and telluro-phosphate [8,9] are thoroughly investigated since the structure of a glass that is formerly used for host-glass is accessible and, according to the study, provides favorable places for cations. Glasses with borosilicate have specific and enhanced qualities, including capacity to transmit UV-NIR, high clarity, mechanical strength, resistance to corrosion, strong chemical stability, high transitional glass temperature and low optical losses in the near and mid-infrared range [10,11]. The main subject of spectroscopic investigations on Ho^{3+} -doped ternary glasses [4,11,12] were fluorescence characteristics of near-infrared and visible wavelength regions. Due to long persistent intermediate metastable levels, the energy levels of the trivalent Ho^{3+} ion are favorable to population inversions ($^5\text{I}_6$, $^5\text{I}_7$). In optical fiber communication, medicines and gas sensors [13], the

2 mg emission corresponding to the $^5I_7 \rightarrow ^5I_8$ transition of the ion Ho^{3+} was utilized [13]. In numerous oxide hosts Ho^{3+} can lead to fascinating light behaviors [3,14–16]. Ho^{3+} states 5S_2 and 5F_5 : oxides have both green and red emissions. The host, temperature and Ho^{3+} concentration are the main determinants of green and red emission intensity. Ho^{3+} : oxides study is also predicated on the promise of a shortwave laser powered by a long wavelength optical pump as a solid-state longitudinal laser [17,18]. Low-phonon amorphous glasses, with rare earth ions, have been said to be very promising in the development of near-infrared laser sources. The glasses exhibit better thermal stability, reduced phonon energy and a decreased OH absorption coefficient with the addition of Holmium ions into the basic composition [17,18]. This leads to a greater stimulated emission cross-section and a longer emission life when rare earth ions undergo a near-infrared laser transition [19,20]. Boro-phosphate glasses are commonly used for the purpose of solid-state lasers and optical fiber amplifier and have a low melting-point. This investigation sought to identify the structural, thermal and optical properties of lithium boro-phosphate glasses, as well as the optimal concentration for future uses in solid-state lasers, for holmium integration and concentration.

2. Experimental

2.1. Synthesis

The traditional melt quenching procedure was used to prepare a set of glasses. The chemical compositions of primed glasses are as follows, $x\text{Li}_2\text{O}-y\text{Bi}_2\text{O}_3-z\text{P}_2\text{O}_5-a\text{Ho}_2\text{O}_3-(1-x-y-z-a)\text{B}_2\text{O}_3$; where $x = 25$ mol%, $y = z = 15$ mol%, a is varied with respect to (45 mol%) B_2O_3 in steps of 0.1, 0.3, 0.5 mol%. For the preceding set of samples, stoichiometric quantities are considered, such as lithium carbonate (Li_2CO_3), bismuth trioxide (Bi_2O_3), ammonium dihydrogen phosphide ($(\text{NH}_4)_2\text{H}_2\text{PO}_4$), holmium trioxide (Ho_2O_3) as rare earth integrated with boric acid. All these chemicals were of AR graded chemicals procured from SRL company, Bangalore, India and used without further purification. These compounds were broken until the homogenous mixture had been reached for 30 min in agate mortar. Following the blend, the porcelain sinker was transferred and held in silted oven in steps of 300°C until it reached 1150°C for 1 h and 30 min to make a homogenous melting. In between the brass moulds, homogenous melt was then quenched for samples called 0, 0.1, 0.3 and 0.5 mol percent of Ho^{3+} dopant concentration, which were called B0H, B01H, B03H and B05H. Care was needed to ensure that the glass samples were not broken during quenching of the hot brass moulds preheated to 200°C . For optical investigations and powder shapes for other research, such as XRD, heat etc., other samples were split into solid pellets.

2.2. Characterization

The prepared B0H set of glass samples were initially analyzed using an X-ray diffractometer (XRD) to validate the amorphous structure using the RIGAKU, ULTIMA IV; 40 kV, 30 mA, which used Cu K radiation with a wavelength of 1.5406 \AA as a source. The refractive index and density of the sample were determined using the Digital Abbe refractometer ATAGO of wavelength 589.3 nm with an accuracy of 0.001 and the Archimedes principle with an immersion liquid toluene ($=0.866 \text{ g/cm}^3$), respectively, after the amorphous structure of the B0H sample set was confirmed. The glass transition temperature of the B0H sample set was determined using DSC analysis, which was carried out using the Mettler instrument; DSC 1 with nitrogen as the atmosphere temperature ranged from RT to 500°C , with a heating rate of 10°C/min . Thermo Nicolet's Avatar 370, with a resolution of 4 cm^{-1} , was utilized as a way to comprehend different modes of vibration in the B0H sample set, which was carried out utilizing the KBR pellet technique and a Fourier transform infrared spectroscope (FTIR). Absorption studies in the UV-Vis-NIR range and photoluminescence studies in the visible region were conducted using a double beam spectrophotometer, Perkin-Elmer Lambda 750, with a resolution of 1 nm, and a spectrofluorometer, Horiba Jobin Yvon fluorolog-3,

both of which used a 450 W source xenon lamp. All of the aforementioned characterizations were completed at room temperature (RT).

3. Results and Discussion

3.1. XRD Analysis

Figure 1 depicts the XRD patterns of the prepared B0H set of samples. All of the XRD patterns show two big humps in the 20° to 60° range in the 2θ range, with no well-crystalline peaks. After and before Ho^{3+} ion doping, the obtained B0H set of samples are non-crystalline in nature.

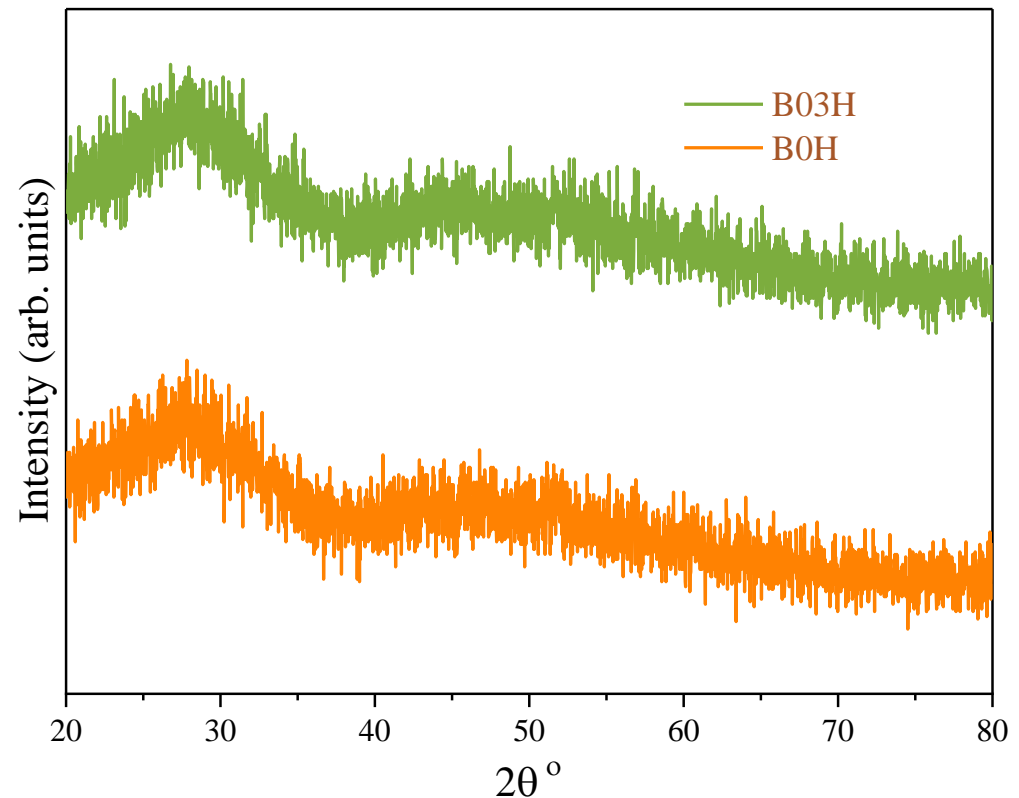


Figure 1. XRD patterns of the Ho doped lithium boro-phosphate glasses.

3.2. Physical Properties with Theoretical Discussion

In order to investigate the effect of Ho^{3+} doping on the physical and optical properties of the prepared glasses, various physical and optical parameters, such as, density, molar volume, average boron-boron separation, packing density, oxygen packing density (OPD), average coordination number, concentration of holmium ions ($C_{\text{Ho}^{3+}}$), holmium inter-ionic distance (r_i), polaron radius (r_p), field strength (F) of holmium field, molar refractivity, polarizability, reflection loss, transmission coefficient, and dielectric constant were evaluated using the various theoretical formulae [18,21–23] and experimentally acquired results.

The estimated values are presented in Table 1. We observed the variation in the values of the density of the B0H set due to the incorporation of Ho^{3+} that was added to the host glass matrix to improve structure compactness, as illustrated in Table 1. Furthermore, holmium molecular weight (377.68 g/mol) differs from borate mass (69.63 g/mol); holmium M.W, in particular, is higher, which results in enhanced formation of non-bridging oxygen's (NBOs). However, in the B0H, the volume of the molar reduces with the increased holmium concentration due to the shrinking bond length. Due to the difference in holmium ionic radii (0.91 Å) and borate (0.27 Å), a variance in the molar volume can also be expected. Further, with increase in the holmium concentration, the $\langle d_{\text{B-B}} \rangle$ also enhanced which supports the variation observed in molar volume. It is found that Li_2O , Bi_2O_3 , B_2O_3 ,

P_2O_5 , and Ho_2O_3 have packing factors of $9.14 \text{ cm}^3/\text{mol}$, $26.28 \text{ cm}^3/\text{mol}$, $20.87 \text{ cm}^3/\text{mol}$, $34.89 \text{ cm}^3/\text{mol}$, and $24.46 \text{ cm}^3/\text{mol}$, respectively. The packing density for the whole B0H set was determined using the packing factor, and the difference in the packing density shows that the oxide glass' rigidity increases as the holmium concentration. The creation of non-bridging oxygen (NBO) after the addition of holmium to the B0H set is explained by OPD variations. The increase in OPD leads to a rise in glass hardness as holmium concentration increases. It is observed that the number of bonds per unit length in the B0H set also decreased as the holmium concentration increased. There is a difference in R_i and an increase in the molecular weight also with the holmium content in the B0H glasses. This has led to the development of a densely packed glass network. We would expect to increase field strength in B0H close to Ho^{3+} ions, as r_p decreases. The results were the same as the estimated values. With holmium concentrations increased greatly, the refractive index of B0H glasses suggested that optical not-linearity was improved in the produced glasses. Thus, effective polarisation and molar repressiveness decreases were found from B01H to B05H. The R_L value of B0H set signified that the low reflection loss resulted in the high transmission coefficient. The conduction width would increase as the holmium concentration in B0H rises. As a result, the metallization requirement is less than 1, implying that the B0H set of materials is insulating [23–25].

Table 1. Summary of various physical and optical parameters obtained from the theoretical and experimental analysis.

Parameters	B0H	B01H	B03H	B05H
ρ	4.041 (1)	3.802 (1)	3.873 (1)	3.934 (1)
t	1.58 (2)	2.03 (3)	1.48 (2)	1.62 (1)
M.W	133.444 (5)	133.760 (5)	134.392 (5)	135.148 (5)
N	1.651 (1)	1.652 (1)	1.653 (1)	1.653 (1)
V_m	33.022 (1)	35.181 (1)	34.699 (1)	34.353 (1)
d_{B-B}	376.121 (1)	383.905 (1)	381.685 (1)	380.000 (1)
V_p	0.631 (1)	0.592 (1)	0.601 (1)	0.607 (1)
OPD	84.790 (1)	79.586 (1)	80.691 (1)	81.504 (1)
CN_{av}	3.850 (6)	3.853 (6)	3.859 (6)	3.871 (6)
n_b	0.702 (1)	0.659 (1)	0.669 (1)	0.678 (1)
$C_{Ho^{3+}}$	-	0.351 (1)	1.067 (1)	1.800 (1)
r_i	-	3.100 (5)	2.140 (5)	1.798 (5)
r_p	-	12.492 (3)	8.628 (3)	7.250 (3)
F	-	1.922 (2)	4.029 (2)	5.707 (2)
R_m	12.059 (1)	12.863 (1)	12.702 (1)	12.576 (1)
α_m	4.780 (1)	5.098 (1)	5.035 (1)	4.984 (1)
R_L (%)	6.030 (1)	6.044 (1)	6.058 (1)	6.058 (1)
ϵ	2.725 (3)	2.729 (3)	2.732 (3)	2.732 (3)
T	0.886 (1)	0.886 (1)	0.885 (1)	0.885 (1)
ϵ_{op}	1.725 (1)	1.729 (1)	1.732 (1)	1.732 (1)
M	0.634 (1)	0.634 (1)	0.633 (1)	0.633 (1)
$\alpha_{o^{2-}}$	1.706 (1)	1.820 (1)	1.798 (1)	1.780 (1)
Λ	0.691 (1)	0.752 (1)	0.741 (1)	0.731 (1)
Λ_{th}	0.810 (4)	0.808 (4)	0.805 (4)	0.804 (4)
X	1.171 (2)	1.327 (2)	1.323 (2)	1.322 (2)
χ_e	0.137 (2)	0.137 (2)	0.137 (2)	0.137 (2)
$\chi^{(3)} \times 10^{-14}$	3.555 (2)	3.582 (2)	3.610 (2)	3.610 (2)

Electronic oxide polarizability can be estimated using experimental refractive index as follows,

$$\alpha_{o^{2-}} = \left[\left(\frac{V_m}{2.52} \right) \left(\frac{n^2 - 1}{n^2 + 2} \right) - \sum \alpha_{cat} \right] / N_{o^{2-}} \text{Å}^3 \quad (1)$$

where, $\sum \alpha_{cat}$ denotes molar cation polarizability and $N_{o^{2-}}$ represents number of oxide ions present in B0H set. For the present B0H set, $a\text{Li}_2\text{O}-b\text{Bi}_2\text{O}_3-c\text{P}_2\text{O}_5-d\text{B}_2\text{O}_3-e\text{Ho}_2\text{O}_3$; $\sum \alpha_{cat}$ can be estimated as $a(2)\alpha_{\text{Li}} + b(2)\alpha_{\text{Bi}} + c(2)\alpha_{\text{P}} + d(2)\alpha_{\text{B}} + e(2)\alpha_{\text{Ho}}$ and $N_{o^{2-}}$ can be estimated as $a(1) + b(3) + c(5) + d(3) + e(3)$. Here $\alpha_{\text{Li}} = 0.0029 \text{Å}^3$, $\alpha_{\text{Bi}} = 1.508 \text{Å}^3$, $\alpha_{\text{P}} = 0.021 \text{Å}^3$, $\alpha_{\text{B}} = 0.003 \text{Å}^3$ and $\alpha_{\text{Ho}} = 0.91 \text{Å}^3$. Also, a, b, c, d and e are mole fractions of respective compounds used in batch calculation.

Furthermore, the optical basicity can be calculated using the expression [23–25],

$$\Lambda = 1.67 \left(1 - \frac{1}{\alpha^{0.2-}} \right) \quad (2)$$

The optical basicity (Λ) is derived from considering theoretical optical basicity (Λ_{th}),

$$\Lambda = \Lambda_{\text{th}} = X_1\Lambda_1 + X_2\Lambda_2 + X_3\Lambda_3 + \dots + X_n\Lambda_n \quad (3)$$

where, $X_{\text{Li}_2\text{O}}$, $X_{\text{Bi}_2\text{O}_3}$, $X_{\text{P}_2\text{O}_5}$, $X_{\text{B}_2\text{O}_3}$ and $X_{\text{Ho}_2\text{O}_3}$ are equivalent mole fractions of different oxides and $\Lambda_{\text{Li}_2\text{O}} = 0.87$, $\Lambda_{\text{Bi}_2\text{O}_3} = 1.19$, $\Lambda_{\text{P}_2\text{O}_5} = 0.33$, $\Lambda_{\text{B}_2\text{O}_3} = 0.42$ and $\Lambda_{\text{Ho}_2\text{O}_3} = 0.945$ are the theoretical basicity of oxides.

Electro negativity (χ) is estimated using the relation,

$$\chi = \frac{\Lambda}{0.75} + 0.25 \quad (4)$$

Electric susceptibility (χ_e) is estimated by a relation,

$$\chi_e = \frac{n^2 - 1}{4\pi} \quad (5)$$

Using Miller's rule, the third order nonlinear optical susceptibility can be predicted as,

$$\chi^{(3)} = [\chi^{(1)}]^4 \times 10^{-10} \text{esu} \quad (6)$$

Figure 2 shows the variation of estimated various physical parameters as a function of Holmium concentration in the B0H set of samples. In the current B0H glass, the oxide ion polarizability rose with increasing holmium content, resulting in more NBO production. To assess the degree of basicity in B0H glass, the optical basicity, which measures the glass's potential to donate the ion's negative charge, was determined. Chemically, glasses having a high electron density would be unstable. The basic nature of the B0H glasses, therefore, means that, with a low level of basicity, the chemistry of the created glasses increases [20–25] as the amount of basicity grows with low electron donations. The theoretical optical basis was further calculated and compared to the empirically measured optical fundamental values. The non-linearity values achieved in B0H were high and, therefore, strongly applicable to non-linear optical systems.

3.3. Glass Transition Temperature

The thermal characteristics of B0H glasses were determined by using a differential scan calorimetry (DSC). DSC may be used to determine glass transition (T_g) temperatures of the B0H. Figure 3 shows B0H and B05H glass samples as a heat flow vs. temperature graph. The T_g in the plot was acquired in the DSC curve as a turning point in the transitional glass area. The T_g decreasing with the insertion of Ho^{3+} ions in the B0H set, which could be caused by the large molar holmium mass, is based on the existing B0H's and B05H samples.

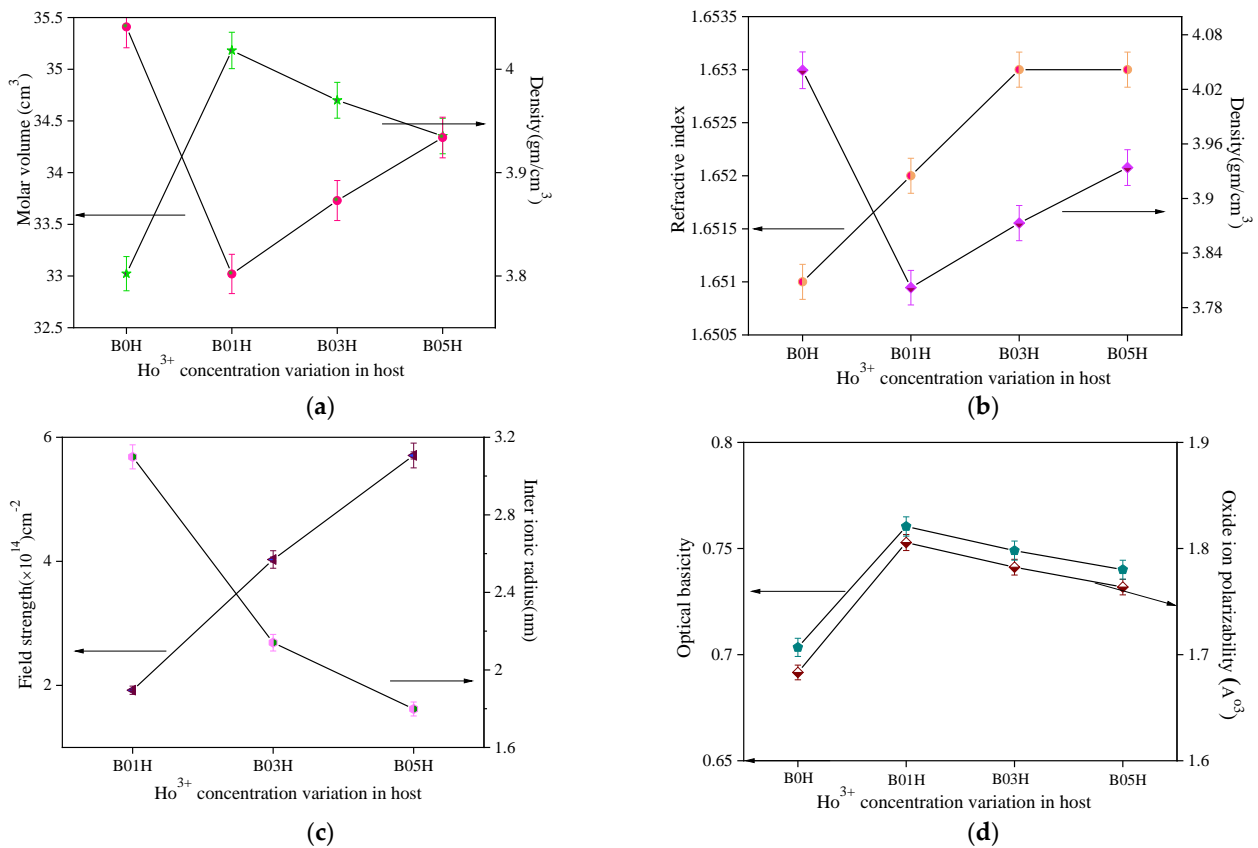


Figure 2. Graphical representation of variation of physical parameters as a function of Ho concentration. (a) is the variation of molar volume and density, (b) is the variation of refractive index and density, (c) variation of field strength and inter ionic radius, (d) is the variation of optical basicity and oxide ion polarizability.

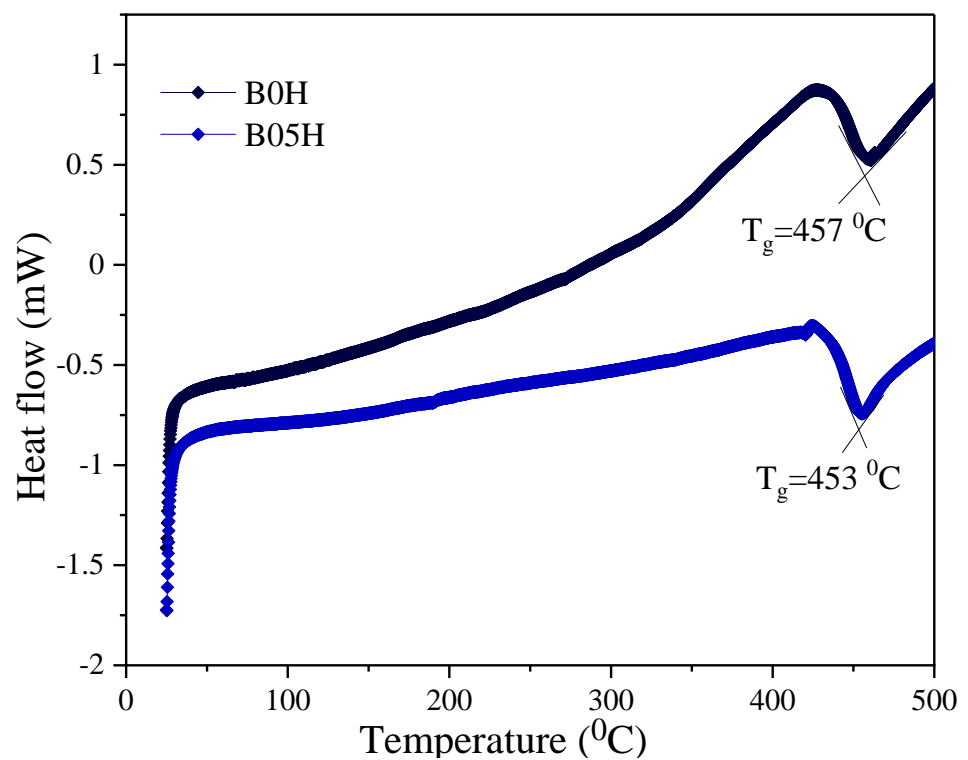


Figure 3. DSC profile of B0H and B05H glass sample.

3.4. Structural Analysis from FTIR Spectroscopy

FTIR was used for structural investigation, and the stacked spectra for the B0H group of materials are shown in Figure 4. The spectra transmittance vs. wavenumber demonstrates that the majority of the vibrations were caused by borate groups. The cage vibration of metal cations such as Bi^{3+} , Li^{+} [26,27] was characterized by three primary bands of $400\text{--}750\text{ cm}^{-1}$, $750\text{--}1200\text{ cm}^{-1}$ and $1200\text{--}1650\text{ cm}^{-1}$ in the region with a weak band of less than 600 cm^{-1} . In the region of $650\text{--}750\text{ cm}^{-1}$, the bending of several borate segments results in a peak. This band has a tiny inclination for moving to a higher wave number called the blue shift. A higher bond strength value reduces the length of bond [18–24]. In this way, Ho increased the structure groups' compactness. The higher concentration in the B0H package caused the rise in density to vary due to the difference in atomic weights of Ho and B. The result was a change in free volume. The outcome was that the band area between 750 and 1200 cm^{-1} was connected with BO_4 deformation and non-bridging oxygen NBO movements. A symmetrical B-O stretching of the BO_3 group was assigned to the region from 1200 to 1650 cm^{-1} . In addition, the BO_4 field was employed to approximate the four-coordinated boron atoms for the bands and BO_3 units [28]. After integration in the B0H host, the production of NBOs was seen. The BO_3 units broke up into BO_4 units that create NBOs, also called dangerous bonds. Figure 5 shows the difference between the four-coordinated boron atoms and the B0H set.

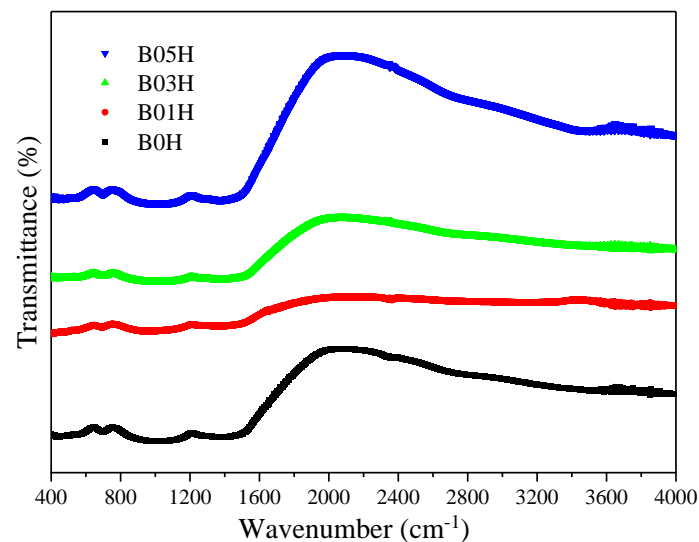


Figure 4. FTIR spectra for B0H set of samples.

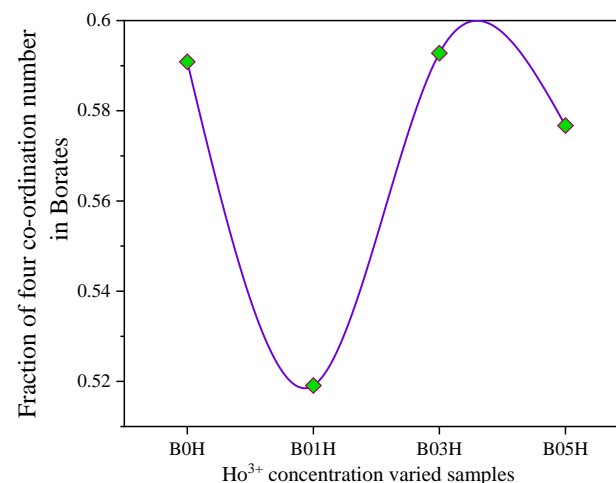


Figure 5. BO_4 fractions in B0H set of samples.

3.5. Optical Properties

For the investigation of optical characteristics, absorption and emission spectra were used. The absorption of the rare earth/dopant (here holmium), depending on the range of UV (ultraviolet) to (near infrared) nitrogen was estimated. The greatest intensity of absorption wavelength in the spectrum was seen for sample B0H spectrum; the same wavelength as excitation wavelength was reported.

3.5.1. UV-Vis-NIR Analysis with Tauc's Plots

Figures 6 and 7 display absorption spectra in the 400–2200 nm range, with transitions numbered. B0H without holmium does not show peaks in Figure 6, but the strength of the peaks grew with the increased concentration of Ho^{3+} -ions in the B0H set. The ground condition ($^5\text{I}_8$) of Ho^{3+} -ions with a 4f transition was detected in seven transitions in the UV-Vis-NIR area, as can be seen in the standard spectra (Figure 7) of the B05H sample. Peak transitions of 417, 450, 486, 538, 642, 1152 and 1948 nm are assigned to $(^5\text{G}, ^3\text{G})_5$, $^5\text{G}_6$, $^5\text{F}_3$, $^5\text{S}_2$, $^5\text{F}_5$, $^5\text{I}_6$ and $^5\text{I}_7$, respectively [13,18,29,30]. Among all transitions, $^5\text{G}_6$ is a hypersensitive transition that is specific to the surrounding atmosphere of the Ho^{3+} -ions; it follows the selection rules $|\Delta S| = 0$, $|\Delta L| \leq 2$ and $|\Delta J| \leq 2$. Electric-dipole interactions cause transitions in the 400–700 nm range, while magnetic-dipole interactions cause transitions around 1950 nm [28–31].

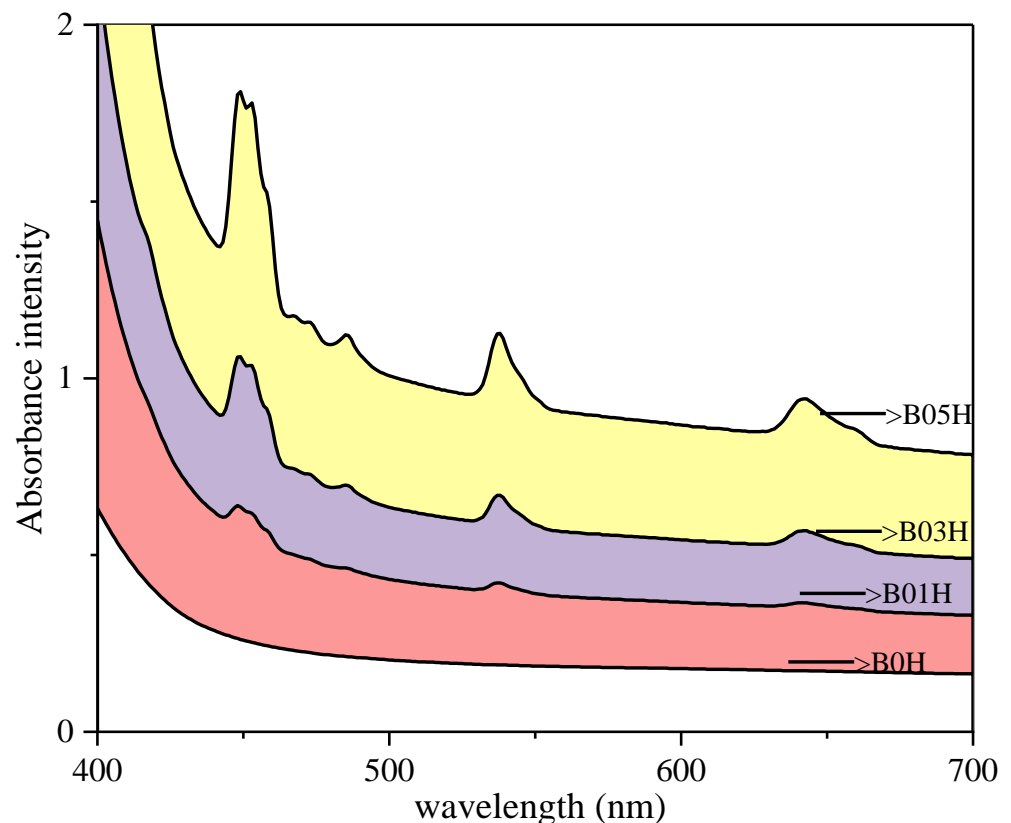


Figure 6. Absorption spectra in UV-Vis region for B0H set.

The absorption co-efficient was estimated using,

$$\alpha(h\nu) = \frac{2.303 \times A}{t} \quad (7)$$

where, A is absorbance recorded for the B0H set and t is the thickness of the B0H set.

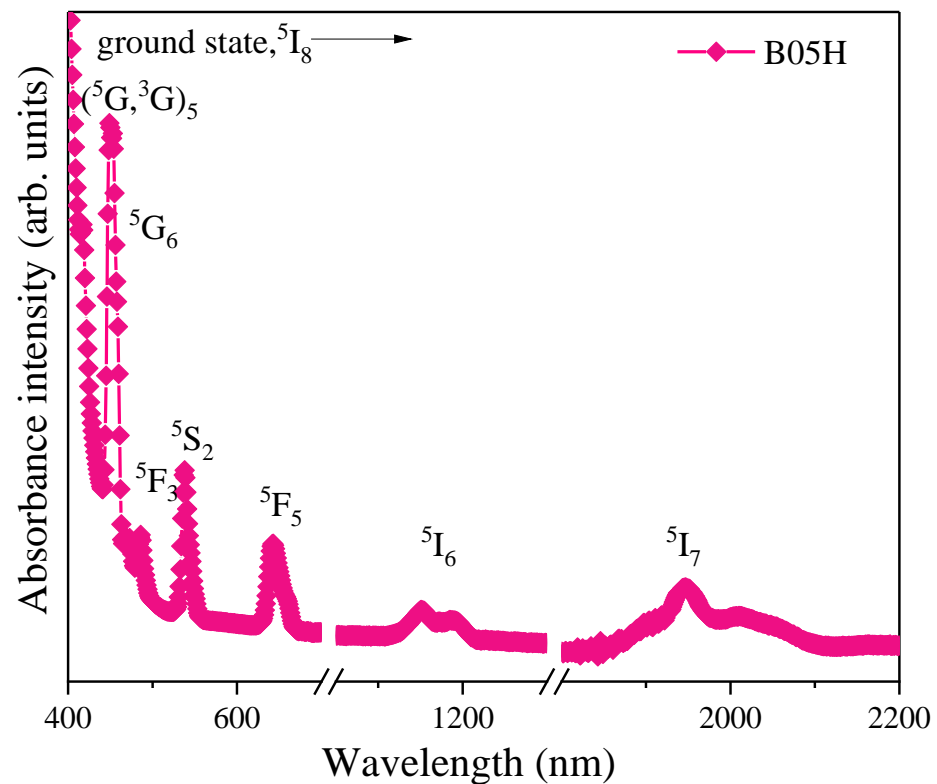


Figure 7. Absorption spectra in UV-Vis-NIR region with assigned transitions for B0H sample.

Details on electronic states may be revealed by the higher energy spectral region, referring to interband electronic transitions. Photon absorption is initially utilized to drive electrons from a full band into an empty band, and the coefficient of absorption increases afterwards. This abrupt change in $\alpha(h\nu)$, and the difference in energy is the resultant energy, is the fundamental absorption edge [32,33]. Davis and Mott suggested a Tauc's [34,35] relation between $\alpha(h\nu)$ and the incident radiations energy (photon energy), which can be expressed as,

$$\alpha(h\nu) = \frac{[t_p (h\nu - E_{g^{opt}})^n]}{h\nu} \quad (8)$$

where t_p is the band tailing parameter (constant), $E_{g^{opt}}$ is the optical band gap energy, and n is depending on the form of transition (direct or indirect). The transitions with $n = 2, 3, 1/2$, and $1/3$ will be indirect allowed, indirect forbidden, direct allowed, and direct forbidden, respectively. This n is often affected by the material's composition, such as crystalline or amorphous. The indirect transition curve is extrapolated in the linear component using photon energy $\nu/s (\alpha h\nu)^{1/2}$ to achieve optical energy gap ($E_{g^{opt}}$) and the estimated values are tabulated in Table 2.

Table 2. Summary of Optical parameter such as Indirect band gap, Urbach energy, Steepness parameter for B0H set of samples.

Samples	Indirect Band Gap (eV) (± 0.01)	Urbach Energy (eV) (± 0.01)	Steepness Parameter (± 0.01)
B0H	2.50	0.34	0.07
B01H	2.89	0.23	0.11
B03H	2.88	0.22	0.11
B05H	2.78	0.26	0.09

Localized states with expanded optical band gaps called exponential tails, also known as Urbach tails, occur in amorphous materials (disordered structure). In an absorption coefficient curve, this tail is above the optical band gap. The Urbach analytical rule [33] expresses the relationship between the absorption co-efficient and photon energy as follows:

$$\alpha(h\nu) = \alpha(h\nu)_0 \exp \frac{h\nu}{\Delta E} \quad (9)$$

Here $\alpha(h\nu)_0$ is a constant and ΔE is known as Urbach energy. The straight-line equation can be obtained by adding logarithm to both sides of the above equation. As a result, ΔE can be determined by plotting the incident photon energy ($h\nu$) versus $\ln\alpha(h\nu)$ and taking the inverse of the straight line's slope. Table 2 shows the predicted values for the B0H set of samples, which corroborate the existence of indirect or phonon-assisted transformations, as well as defects caused by the presence of Ho^{3+} -ions in B0H glass. ΔE stands for structural stability and the lower the ΔE , the greater the structural stability [36–38]. The steepness parameter (S) [39] represents the relaxation of the exciton—phonon due to the expansion of optical absorption. This can be determined using the formula:

$$S = \frac{kT}{\Delta E} \quad (10)$$

where, k is Boltzmann constant, T is the room temperature and ΔE is Urbach energy.

A lower S value suggests that temperature was less of a consideration. Table 2 summarizes the results. Figure 8 depicts an indirect energy (Tauc's) and the Urbach energy plots.

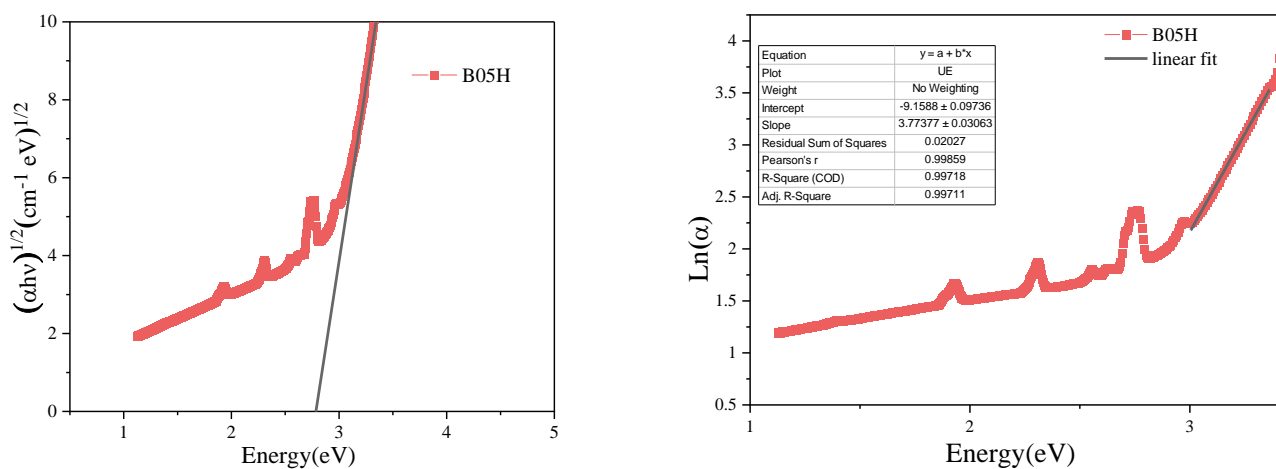


Figure 8. Indirect band gap (left) and Urbach energy (right) plots.

3.5.2. Photoluminescence and CIE Diagram

The emission spectra in the visible field were recorded using excitation wavelengths of 450 and 550 nm. The transition states and their spectra are depicted in Figure 9. Similar transitions can be detected in emission spectra with an excitation wavelength of 450 nm, whereas spectra with an excitation wavelength of 550 nm show a significant peak around 600 nm. Because of the spectral overlap in the host, 0.3 mol% in B0H indicates a higher intensity of the ${}^5\text{F}_5\text{--}{}^5\text{I}_8$ transition [29–31].

To validate the emission color acquired for the B0H collection, the CIE (Commission International de l'Eclairage) coordinates diagram was plotted (Figure 10) using the emission data supplied. Table 3 illustrates the findings of applying the CIE 1931 chromaticity diagram [40] and the McCamy analytical formula for CCT (correlated color temperature) [41] under 450 and 550 nm excitation, which are corroborated by (x, y) co-ordinate values. Based on the applications [42], we will customize the host to have a desired emission color. The results show that, when the prepared B0H set of glasses was excited at 550 nm, it emitted

orange red light and, when excited at 450 nm, it emitted near-white light. This shows that the produced samples could be used in near-infrared light emission applications.

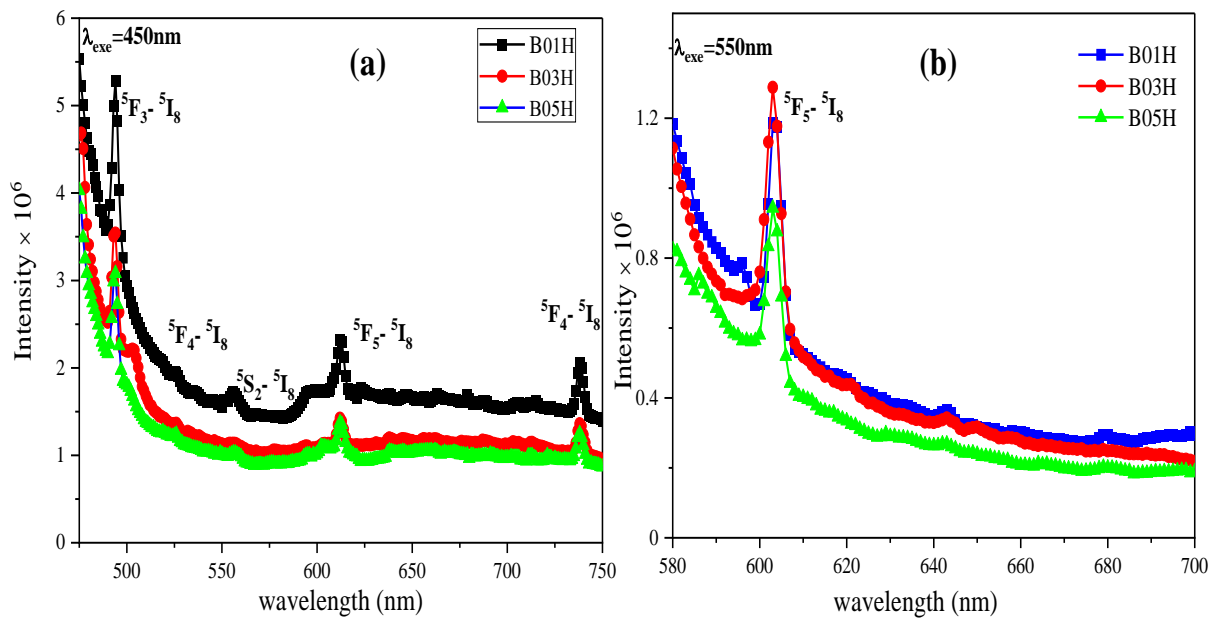


Figure 9. Emission spectra of B0H set sample for (a) 450 and (b) 550 nm excitation.

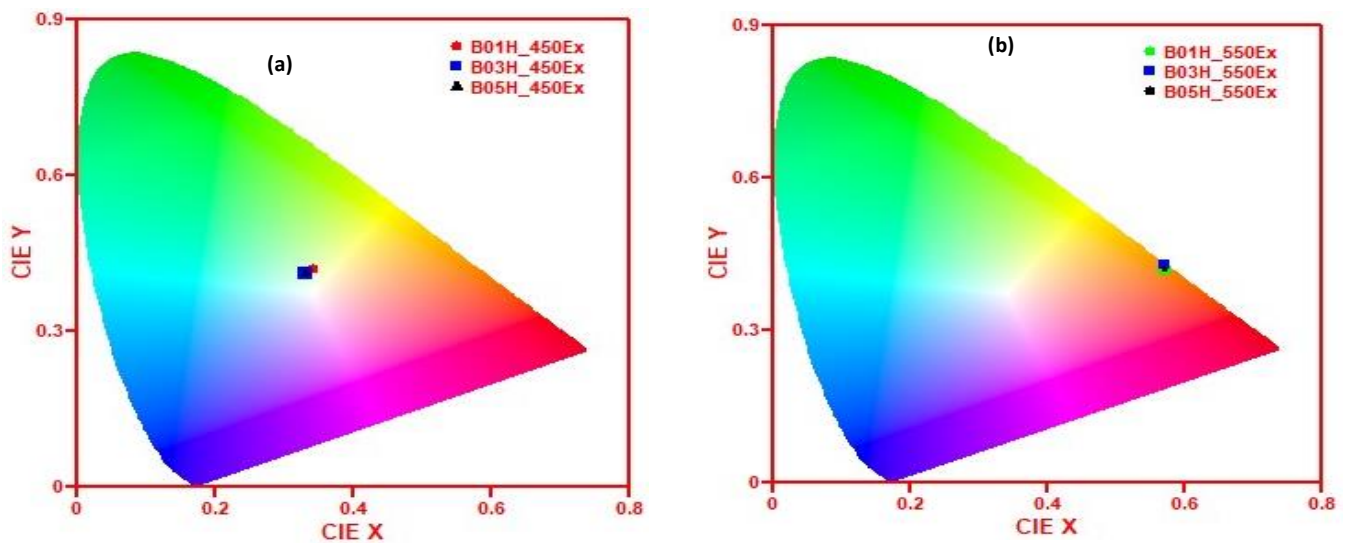


Figure 10. CIE diagram of B0H set for (a) 450 nm and (b) 550 nm excitation.

Table 3. CIE co-ordinates and CCT values.

Sample	Excitation Wavelength (nm)	(x, y) Co-Ordinates	Emission Colour	CCT (K)
B01H	450	(0.34, 0.42)	Yellowish white	5287 (cool)
B03H	450	(0.33, 0.41)	Yellowish white	5578 (cool)
B05H	450	(0.33, 0.41)	Yellowish white	5578 (cool)
B01H	550	(0.57, 0.42)	Reddish-orange	1805
B03H	550	(0.57, 0.43)	Reddish-orange	1846
B05H	550	(0.58, 0.42)	Reddish-orange	1771

4. Conclusions

Holmium-doped heavy metal oxide incorporated lithium boro-phosphate glasses were prepared using the standard melt quenching convention technique. XRD analysis confirmed the amorphous structure of the novel holmium inclusion heavy metal oxide containing lithium boro-phosphate glasses. Density increases with holmium addition reflect holmium's larger molecular weight than borate, which is well supported by DSC and FTIR experiments. The present glasses' third-order non-linearity values were high, indicating that they should be employed in non-linear optical systems. Absorption investigations in the UV-Vis-NIR region revealed seven transitions, including the hypersensitive transition (5G_6). As the holmium concentration in the glasses grew, the Urbach energy, or steepness parameter, represented glass stability. The emission profile of glasses for 450 and 550 nm excitations was evaluated in terms of emission wavelength and intensity for both concentrations of holmium-doped glasses. As a result of the spectral overlap in the host, 0.3 mol% for 550 nm excitation displays the maximum intensity in the $^5F_5 \rightarrow ^5I_8$ transition. According to the CIE chromaticity diagram, the emission of all the glass samples was yellowish-white and reddish-orange for two excitations that are substantially closer to the white light emission zone. According to McCamy CCT, the current glasses are suited for solid state laser applications with 450 nm excitation. It's also worth noting that the physical, structural, thermal, and optical properties of today's glasses are all intrinsically correlated.

Author Contributions: Data curation, S.A.A., M.O.A., A.A., M.S., N.P., R.D. and S.F.A.; Formal analysis, S.A.A., A.A., M.S., N.P. and R.D.; Funding acquisition, M.O.A., A.A. and S.F.A.; Investigation, S.A.A., M.O.A., A.A., N.P., R.D. and S.F.A.; Methodology, S.A.A. and M.O.A.; Resources, M.S., N.P., R.D. and S.F.A. All authors have read and agreed to the published version of the manuscript.

Funding: This Project was funded by the Deanship of Scientific Research (DSR), King Abdulaziz University, Jeddah.

Institutional Review Board Statement: Not applicable.

Informed Consent Statement: Not applicable.

Data Availability Statement: Not applicable.

Acknowledgments: This Project was funded by the Deanship of Scientific Research (DSR), King Abdulaziz University, Jeddah, under grant No. (KEP-1-194-40). The authors, therefore, acknowledge with thanks DSR technical and financial support.

Conflicts of Interest: The authors declare no conflict of interest.

References

1. Zakery, A.; Elliott, S.R. Optical properties and applications of chalcogenide glasses: A review. *J. Non Cryst. Solids* **2003**, *330*, 1–12. [[CrossRef](#)]
2. Knowles, J.C. Phosphate based glasses for biomedical applications. *J. Mater. Chem.* **2003**, *10*, 2395–2401. [[CrossRef](#)]
3. Mariselvam, K.; Liu, J. Green emission and laser properties of Ho³⁺ doped titano lead borate (TLB) glasses for colour display applications. *J. Solid State Chem.* **2021**, *293*, 121793. [[CrossRef](#)]
4. Alqarni, A.S.; Hussain, R.; Ghoshal, S.K.; Alamri, S.N.; Yamusa, Y.A.; Jupri, S.A. Intense red and green luminescence from holmium activated zinc-sulfo-boro-phosphate glass: Judd-Ofelt evaluation. *J. Alloys Compd.* **2019**, *808*, 151706. [[CrossRef](#)]
5. Lakshminarayan, G.; Baki, S.O.; Lira, A.; Caldino, U.; Rocha, A.N.M.; Kityk, I.V.; Abas, A.F.; Alresheedi, M.T.; Mahdi, M.A. Effect of alkali/mixed alkali metal ions on the thermal and spectral characteristics of Dy³⁺: B²O³-PbO-Al²O³-ZnO glasses. *J. Non Cryst. Solids* **2018**, *481*, 191–201. [[CrossRef](#)]
6. Yu, H.; Xin, R.; Zhang, X.; Liu, H.; Zheng, K.; Zhao, J.; Zhan, L.; Xu, C.; Wan, W.; Zhu, Y.; et al. Crystallization behavior, quantitation of Ce³⁺/Ce⁴⁺ and chemical stability analysis of multiple alkaline earths borosilicate glasses for immobilizing simulated tetravalent actinides. *J. Non Cryst. Solids* **2021**, *558*, 120642. [[CrossRef](#)]
7. Reddy, B.N.K.; Raju, B.D.; Thyagarajan, K.; Ramanaiah, R.; Jho, Y.-D.; Reddy, B.S. Optical characterization of Eu³⁺ ion doped alkali oxide modified borosilicate glasses for red laser and display device applications. *Ceram. Int.* **2017**, *43*, 8886–8892. [[CrossRef](#)]
8. Shen, X.; Cheng, G.; Zhang, L.; Wei, W. Fabrication of a hybrid-cladding tellurite glass fiber doped with Tm³⁺ and Ho³⁺. *J. Lumin.* **2020**, *227*, 117540. [[CrossRef](#)]
9. Bulus, I.; Hussain, R.; Ghoshal, S.K.; Tamuri, A.R.; Danmallam, I.M.; Yamusa, Y.A. Europium-doped boro-telluro-dolomite glasses for red laser applications: Basic insight into spectroscopic traits. *J. Non Cryst. Solids* **2020**, *534*, 119949. [[CrossRef](#)]

10. Benouila, O.; Aiadi, K.E.; Rehouma, F.; Poulain, M.; Benhbirech, F. Thermal stability and spectroscopic study of Ho³⁺/Yb³⁺ co-doped fluorophosphates glasses. *J. King Saud Univ. Sci.* **2019**, *31*, 628–634. [[CrossRef](#)]
11. Jimenez, J.A. Spectroscopic investigation of the influence of Cu⁺ ions and plasmonic Cu particles on Ho³⁺ luminescence in phosphate glass. *Chem. Phys.* **2021**, *541*, 111045. [[CrossRef](#)]
12. Li, B.; Zhao, X.; Pun, E.Y.B.; Lin, H. Upconversion photon quantification of Ho³⁺ in highly transparent fluorotellurite glasses. *Opt. Laser Technol.* **2018**, *107*, 8–14. [[CrossRef](#)]
13. Kochanowicz, M.; Zmojda, J.; Miluski, P.; Baranowska, A.; Ragin, T.; Dorosz, J.; Kuwik, M.; Pisarski, W.A.; Pisarska, J.; Lesniak, M.; et al. 2 μm emission in gallo-germanate glasses and glass fibers co-doped with Yb³⁺/Ho³⁺ and Yb³⁺/Tm³⁺/Ho³⁺. *J. Lumin.* **2019**, *211*, 341–346. [[CrossRef](#)]
14. Sobczyk, M.; Marek, L. Comparative study of optical properties of Ho³⁺-doped RE²O³-Na²O-ZnO-TeO² glasses. *J. Lumin.* **2019**, *206*, 308–318. [[CrossRef](#)]
15. Wan, Z.; Li, W.; Mei, B.; Liu, Z.; Yang, Y. Fabrication and spectral properties of Ho-doped calcium fluoride transparent ceramics. *J. Lumin.* **2020**, *223*, 117188. [[CrossRef](#)]
16. Kochanowicz, M.; Zmojda, J.; Muluski, P.; Baranowska, A.; Kuwik, M.; Pisarski, W.A.; Pisarska, J.; Dorosz, J.; Dorosz, D. Sensitization of Ho³⁺-doped fluoroindate glasses for near and mid-infrared emission. *Opt. Mater.* **2020**, *101*, 109707. [[CrossRef](#)]
17. Prasad, T.J.; Neelima, G.; Ravi, N.; Kiran, N.; Reddy, N.N.K.; Kummara, V.K.; Suresh, K.; Gadige, P. Optical and spectroscopic properties of Ho³⁺-doped fluorophosphate glasses for visible lighting applications. *Mater. Res. Bull.* **2020**, *124*, 110753.
18. Rani, P.R.; Venkateshwarlu, M.; Swapna, K.; Mahamuda, S.K.; Prasad, M.V.V.K.S.; Rao, A.S. Spectroscopic and luminescence properties of Ho³⁺ ions doped Barium Lead AluminoFluoro Borate glasses for green laser applications. *Solid. Stat. Sci.* **2020**, *102*, 106175. [[CrossRef](#)]
19. Chen, Q.; Li, Z.; Miao, B.; Ma, Q. Thermal, nonlinear, magnetic and faraday rotation properties of sol-gel diamagnetic glass/NaYF₄: Fe, Ho³⁺: Role of magnetic ions. *J. Alloys Compd.* **2021**, *858*, 157631. [[CrossRef](#)]
20. Madhu, A.; Eraiah, B.; Manasa, P.; Srinatha, N. Nd³⁺-doped lanthanum lead boro-tellurite glass for lasing and amplification applications. *Opt. Mater.* **2018**, *75*, 357–366. [[CrossRef](#)]
21. Hemalatha, S.; Nagaraja, M.; Madhu, A.; Suresh, K.; Srinatha, N. The role of Sm²O₃ on the structural, optical and spectroscopic properties of multi-component ternary borate glasses for orange-red emission applications. *J. Non Cryst. Solids* **2021**, *554*, 120602. [[CrossRef](#)]
22. James, J.T.; Jose, J.K.; Manjunatha, M.; Suresh, K.; Madhu, A. Structural, luminescence and NMR studies on Nd³⁺-doped sodium-calcium-borate glasses for lasing applications. *Ceram. Inter.* **2020**, *46*, 27099–27109. [[CrossRef](#)]
23. Algradee, M.A.; Sultan, M.; Samir, O.M.; Alwany, A.E.B. Electronic polarizability, optical basicity and interaction parameter for Nd₂O₃ doped lithium-zinc-phosphate glasses. *J. Appl. Phys.* **2017**, *6*, 163–170.
24. Nanda, K.; Berwal, N.; Kundu, R.S.; Punia, R.; Kishore, N. Effect of doping of Nd³⁺ ions in BaO-TeO₂-B₂O₃ glasses: A vibrational and optical study. *J. Mol. Struct.* **2015**, *1088*, 147–154. [[CrossRef](#)]
25. Tasheva, T.R.; Dimitrov, V.V. Synthesis, structure and nonlinear optical properties of tellurium oxide-bismuth oxide-boron oxide glasses. *Bulg. Chem. Commun.* **2017**, *49*, 43–48.
26. Madhu, A.; Eraiah, B.; Manasa, P.; Basavapoornima, C. Er³⁺-ions doped lithium-bismuth-boro-phosphate glass for 1532 nm emission and efficient red emission up conversion for telecommunication and lasing applications. *J. Non Cryst. Solids* **2018**, *495*, 35–46. [[CrossRef](#)]
27. Pisarski, W.A.; Goryczka, T.; Wodecka-Dus, B.; Plonska, M.; Pisarska, J. Structure and properties of rare earth-doped lead borate glasses. *Mater. Sci. Eng. B* **2005**, *122*, 94–99. [[CrossRef](#)]
28. Madhu, A.; Eraiah, B. The structural studies of vanadium substituted lithium-bismuth-boro-tellurite glass. *AIP Conf. Proc.* **2018**, *1953*, 090056.
29. Pisarska, J.; Kuwik, M.; Górny, A.; Kochanowicz, M.; Zmojda, J.; Dorosz, J.; Dorosz, D.; Sitarz, M.; Pisarski, W.A. Holmium doped barium gallo-germanate glasses for near-infrared luminescence at 2000 nm. *J. Lumin.* **2019**, *215*, 116625. [[CrossRef](#)]
30. Jupri, S.A.; Ghoshal, S.K.; Omar, M.F.; Yusof, N.N. Spectroscopic traits of holmium in magnesium zinc sulfophosphate glass host: Judd-Ofelt evaluation. *J. Alloys Compd.* **2018**, *753*, 446–456. [[CrossRef](#)]
31. Prasad, V.R.; Damodaraiah, S.; Ratnakaram, Y.C. Optical spectroscopy and luminescence properties of Ho³⁺ doped zinc fluorophosphate (ZFP) glasses for green luminescent device applications. *Opt. Mater.* **2018**, *78*, 63–71. [[CrossRef](#)]
32. Ikhmayies, S.J.; Ahmad-Bitar, R.N. A study of the optical bandgap energy and Urbach tail of spray-deposited CdS: In thin films. *J. Mater. Res. Technol.* **2013**, *2*, 221–227. [[CrossRef](#)]
33. Urbach, F. The Long-Wavelength Edge of Photographic Sensitivity and of the Electronic Absorption of Solids. *Phys. Rev.* **1953**, *92*, 1324. [[CrossRef](#)]
34. Davis, E.A.; Mott, N.F. Conduction in non-crystalline systems V. Conductivity, optical absorption and photoconductivity in amorphous semiconductors. *Philos. Mag.* **1970**, *22*, 903–922. [[CrossRef](#)]
35. Tauc, J.; Grigorovice, R.; Vancu, A. Optical properties and electronic structure of amorphous germanium. *Phys. Status Solidi B* **1966**, *15*, 627–637. [[CrossRef](#)]
36. Redfield, D. Effect of defect fields on the optical absorption edge. *Phys. Rev.* **1963**, *130*, 916. [[CrossRef](#)]
37. Weinstein, I.A.; Zatsépin, A.F.; Kortov, V.S. Effects of structural disorder and Urbach's rule in binary lead silicate glasses. *J. Non Cryst. Solids* **2001**, *279*, 77. [[CrossRef](#)]

38. Fuxi, G. *Optical and Spectroscopic Properties of Glass*; Springer: Berlin/Heidelberg, Germany, 1962.
39. Mahr, H. Ultraviolet Absorption of KI Diluted in KCl Crystals. *Phys. Rev.* **1962**, *125*, 1510–1516. [[CrossRef](#)]
40. Schubert, F. *Light-Emitting Diodes*, 2nd ed.; Cambridge University Press: Cambridge, UK, 2006; Chapter 17; p. 292.
41. McCamy, C.S. Correlated color temperature as an explicit function of chromaticity coordinates. *Color Res. Appl.* **1992**, *17*, 142–144. [[CrossRef](#)]
42. Erdem, T.; SNizamoglu Sun, X.W.; Demir, H.V. A photometric investigation of ultra-efficient LEDs with high color rendering index and high luminous efficacy employing nanocrystal quantum dot luminophores. *Opt. Express* **2010**, *18*, 340–347. [[CrossRef](#)]